Tracing Cationic Nutrients from Xylem into Stem Tissue of French Bean by Stable Isotope Tracers and Cryo-Secondary Ion Mass Spectrometry[W][OA]

Ralf Metzner*, Heike Ursula Schneider, Uwe Breuer, Michael Robert Thorpe, Ulrich Schurr, and Walter Heinz Schroeder

Central Division of Analytical Chemistry (R.M., U.B.) and Phytosphere Institute (ICG-3) (R.M., H.U.S., M.R.T., U.S., W.H.S.), Forschungszentrum Jülich, 52425 Juelich, Germany

Fluxes of mineral nutrients in the xylem are strongly influenced by interactions with the surrounding stem tissues and are probably regulated by them. Toward a mechanistic understanding of these interactions, we applied stable isotope tracers of magnesium, potassium, and calcium continuously to the transpiration stream of cut bean (*Phaseolus vulgaris*) shoots to study their radial exchange at the cell and tissue level with stem tissues between pith and phloem. For isotope localization, we combined sample preparation with secondary ion mass spectrometry in a completely cryogenic workflow. After 20 min of application, tracers were readily detectable to various degrees in all tissues. The xylem parenchyma near the vessels exchanged freely with the vessels, its nutrient elements reaching a steady state of strong exchange with elements in the vessels within 20 min, mainly via apoplastic pathways. A slow exchange between vessels and cambium and phloem suggested that they are separated from the xylem, parenchyma, and pith, possibly by an apoplastic barrier to diffusion for nutrients (as for carbohydrates). There was little difference in these distributions when tracers were applied directly to intact xylem via a microcapillary, suggesting that xylem tension had little effect on radial exchange of these nutrients and that their movement was mainly diffusive.

Long-distance transport of nutrients in stems is strongly influenced by the interaction of the moving xylem sap with the surrounding tissues (e.g. phloem; Stout and Hoagland, 1939; Biddulph and Markle, 1944). The importance of this radial exchange was highlighted in studies on budgets of carbon/nitrogen and mineral nutrients (Pate et al., 1979; Jeschke et al., 1985, 1991; Wolf et al., 1991). The composition of a solution is changed during perfusion of stem pieces (Gilmer and Schurr, 2007), suggesting that xylem sap composition is regulated. Thus, the fluxes of nutrients in the xylem could be regulated through the ionic concentration and also from the influence of nutrient concentration (e.g. potassium) on hydraulic properties (Thompson and Zwieniecki, 2005). The transport of these nutrients in stems, therefore, does not occur in a simple pipeline connecting roots with leaves but in pathways that involve many tissues in the stem, in the same way that photoassimilate transport is not confined to sieve tubes (van Bel, 2003). However, perfusion experiments with stem pieces may be inappropriate for elucidating these interactions (van Ieperen, 2007), since lateral flow may be promoted by the unnatural pressure regime. This reservation also applies when the root pressure chamber is used to extract sap, for example, in experiments that showed strong interactions between xylem and adjacent tissues (Siebrecht et al., 2003; Gilmer and Schurr, 2007). Therefore, studies of nutrient and water movement in the xylem should use techniques that minimize any perturbation of the water status of all stem tissues.

Isotope tracers are ideal for studies toward a mechanistic understanding of nutrient exchange between the transpiration stream and different stem tissues, because they are chemically identical to the traced elements. Enriched stable isotopes are available for most nutrients and can be detected at subcellular spatial resolution with imaging mass spectrometric techniques such as secondary ion mass spectrometry (SIMS), provided that the distribution of diffusible tracers can be preserved until completion of the analysis. Strict cryogenic sample preparation followed by analysis with SIMS below −130°C (cryo-SIMS) has been shown to satisfy this criterion (Metzner et al., 2008), with scanning electron microscopy of the frozen samples (cryo-SEM) for quality control and detailed anatomical information of the individual tissues.

Here, we used this cryogenic protocol to examine the exchange between xylem vessels and stem tissue of French bean (*Phaseolus vulgaris* 'Fardenlosa Shiny'), with stable isotope tracers for potassium, calcium, and magnesium applied to the transpiration stream of a cut

* Corresponding author; e-mail r.metzner@fz-juelich.de.

The author responsible for distribution of materials integral to the findings presented in this article in accordance with the policy described in the Instructions for Authors (www.plantphysiol.org) is: Ralf Metzner (r.metzner@fz-juelich.de).

[W] The online version of this article contains Web-only data.

[OA] Open Access articles can be viewed online without a subscription.

www.plantphysiol.org/cgi/doi/10.1104/pp.109.143776

shoot. Based on earlier microanalytical studies on the diffusion kinetics of cationic nutrients moving into roots (Kuhn et al., 2000; Horst et al., 2007), we selected two different periods of tracer application, namely 20 min to show any potential diffusion barriers and 240 min to show distribution patterns after reaching a steady state in nutrient exchange between xylem and surrounding tissue. We evaluated our standard method of tracer application, via the cut stem, in which stem water status was disturbed, in an ancillary experiment where the solution entered via microcapillary directly into xylem under tension.

RESULTS

Tracer solutions, with stable isotopes of naturally minor abundance of magnesium, potassium, and calcium (^{26}Mg, ^{41}K, and ^{44}Ca, respectively) highly enriched to greater than 94% total element, contained 2.5 mM of each of the three elements. Solution entered the cut transpiring shoot (Supplemental Fig. S1 shows the setup) until samples were excised from the first internode above the primary leaves, approximately 25 cm from the application site. They were immediately shock frozen to preserve diffusible ion distribution.

The high quality of tissue preservation is demonstrated by the cryo-SEM image of a cryo-planed surface after cryo-SIMS analysis and freeze etching (Fig. 1A). Such cryo-SEM images helped in assigning the cryo-SIMS signals to the individual structures. Stained cross-sectional light micrographs (Fig. 1B) also helped to identify tissues.

Tracer Signal Distribution after 20 min

Cryo-SIMS maps at high mass resolution give unambiguous identification of the individual isotopes in an image of 500 × 500 μm^2 with a spatial resolution of 10 to 7 μm. In these isotope maps, signal (S^I, counts of isotope I per pixel) shows isotope from both the plant (at natural abundance) and also from the tracer solution. Taking potassium as an example, potassium from the plant is at natural abundance (6.7% ^{41}K and 93.3% ^{39}K). The tracer solution, in contrast, contains more than 94% ^{41}K and less than 6% ^{39}K (Table I). An S^{39K} image, therefore, contains both plant-originating and tracer-originating S^{39K}, and similarly for the corresponding S^{41K} image. Another issue for interpreting the data is that the signal may not show concentrations because signal generation (i.e. ionization) depends on the specific element imaged (e.g. higher for potassium than for calcium), and the local ionization depends on the matrix, the immediate atomic vicinity of the analyte, and this region will be particularly inhomogeneous for biological tissues. Nevertheless, signals from isotopes of the same element are equally influenced by the matrix, so if the image patterns for an element's isotopes are not the same, it is obvious where tracer is present. Tracer presence can be calculated everywhere from the divergence of the isotope ratio from the natural abundance (see below). For assignment of isotope signal to tissue structure, isotope maps (Fig. 2), were laid over the corresponding cryo-SEM image (Fig. 1A).

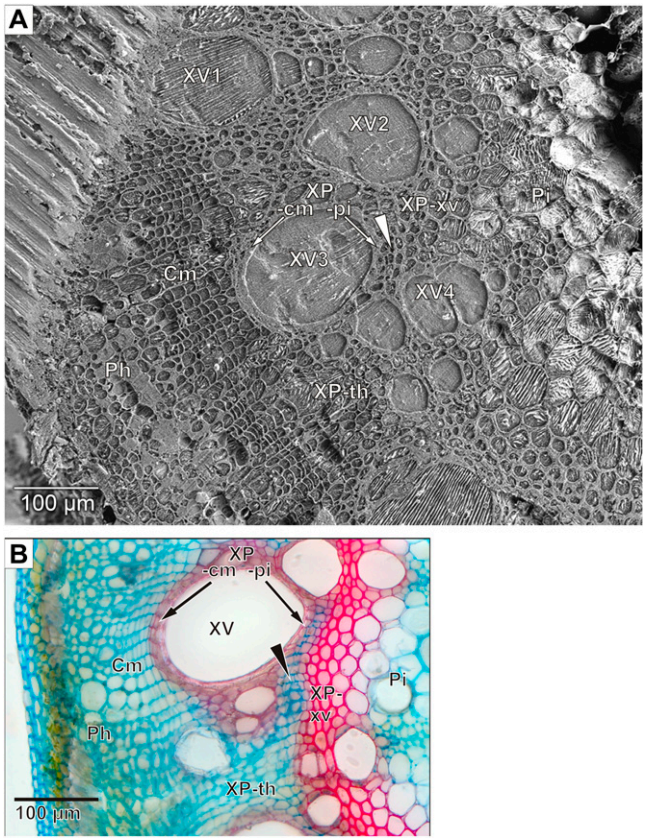

Figure 1. Cross-sectional anatomy of the French bean stem. A, Tissue structures revealed in cryo-SEM by freeze etching the surface after the sample has been analyzed by cryo-SIMS. Xylem vessels (XV1–XV4) and two types of xylem parenchyma are visible that differ by their cell wall morphology. Thick-walled xylem parenchyma is composed of two subtypes, the small and weakly vacuolated cells enclosing the vessels in the shape of an axial sheath (subdivided for measurement purposes into half sheaths facing pith and cambium: XP-pi and XP-cm) and the larger and strongly vacuolated cells between the vessels (XP-xv). Thin-walled xylem parenchyma (XP-th) occurs between the cambium and the thick-walled xylem parenchyma. There are also islands of thin-walled xylem parenchyma (XP-is; arrowhead) within the thick-walled xylem parenchyma. Xylem is bordered toward the hollow center of the stem by the pith (Pi). Toward the stem periphery are the cambium (Cm) and phloem (Ph). On the top left is tissue and water that had not been cryo-planed. B, Light microscopic image of a hand section of a comparable tissue area. Double staining was with astra-blue (cellulose cell walls stain blue) and safranin (lignified cell walls stain red).

The two isotope maps for all three elements differ, showing that all tracers are present in the tissues. Concerning magnesium, with ^{26}Mg as tracer, the highest S^{24Mg} values occurred in a distinct area of thin-walled xylem parenchyma (Fig. 2A, bottom right), in parts of the thick-walled xylem parenchyma from the vessels toward the pith, and in part of the phloem. The

Table I. *Isotopic composition of the applied tracer solution and of unlabeled solution*

The abundances were calculated from three SIMS measurements of air-dried drops of solution on silicon substrate (Eq. 2) and presented as mean percentages ± 2σ (n = 3). The reference literature data are taken from Böhlke et al. (2005). Two different batches of potassium tracer were used in the four types of experiments, as listed in Table II.

Isotopes	^{24}Mg	^{25}Mg	^{26}Mg
Magnesium isotopes			
Tracer	2.0 ± 0.2	1.0 ± 0.2	97.0 ± 0.2
Unlabeled	79.1 ± 2.4	9.6 ± 1.4	12.8 ± 2.4
Literature	79.0	10.0	11.0
	^{39}K	^{41}K	
Potassium isotopes			
Tracer experiment 1	2.9 ± 0.6	97.1 ± 0.6	
Tracer experiments 2, 3, 4	5.5 ± 0.6	94.5 ± 0.6	
Unlabeled	93.7 ± 1.0	6.3 ± 1.0	
Literature	93.3	6.7	
	^{40}Ca	^{44}Ca	
Calcium isotopes			
Tracer	3.2 ± 2.6	96.7 ± 2.6	
Unlabeled	97.8 ± 0.2	2.2 ± 0.2	
Literature	96.9	2.1	

highest S^{26Mg} values occurred in thick-walled xylem parenchyma cells enclosing the vessels and neighboring thick-walled xylem parenchyma facing the pith (Fig. 2B). Both potassium isotope images (Fig. 2, C and D) showed high signal throughout the area of thick-walled xylem parenchyma. Slight differences are indicated for the pith and some restricted regions of thick-walled xylem parenchyma between the metaxylem vessels. For calcium, there are prominent differences between the two images (Fig. 2, E and F): S^{40Ca} and S^{44Ca} were both high in thick-walled xylem parenchyma, but S^{40Ca} maxima were both in the pith and in phloem "hot spots." These isotope maps are representative of 10 samples from nine plants. The tracer solution uptake rate of approximately 0.2 mL min^{-1} resembled the transpiration rate of uncut control plants and, with a xylem vessel volume of 46 ± 19 μL (measured by centrifugation; n = 7), would have replaced the sap 87-fold. Thus, the solution would have arrived at the sampling site by plug flow after about 15 s, and with handling time this would be 30 s after cutting the stem.

Tracer Fractions after 20 min

The isotope maps (Fig. 2) show tracer signal in the vessels and many tissues in the stem cross-section after 20 min of uptake of tracer solution, but the images of tracer isotope could reflect natural element where the local concentration was high enough, even though the natural abundance of the tracer isotopes is low. This problem, and that of matrix effects, was resolved by calculating F_E, the fraction of element E originating from the tracer solution (see "Materials and Methods," Eq. 1). F_E is zero where tracer isotope has natural abundance and 100% where isotopic composition is the same as the applied tracer solution, so that contrast in the F_E images shows local differences in the fractions.

At 20 min, there were large fractions of all tracers in the vessel lumina (Fig. 3, B–D) and tracers had obviously spread into the surrounding tissues (identified by an anatomical map; Fig. 3A). Potassium F_K values were clearly lower outside the vessels, but magnesium F_{Mg} was only a little lower and calcium F_{Ca} was similar to the vessel lumina in nearly all the xylem parenchyma. The pith, phloem, and cambium showed markedly lower tracer fractions compared with the xylem parenchyma. Often, a vessel (Figs. 1A, XV1, and 3A, asterisk) displayed negligible tracer fractions for all three elements. These vessels also showed higher ^{39}K but lower ^{41}K signals than other vessels (Fig. 2, C and D), suggesting that they were nonconducting and probably immature. Fractions (F) for various regions of interest (ROI) were calculated from the total signal in each region, and mean values from three replicates are shown in Figure 4. In vessel lumina, all values were significantly below 100% (Fig. 4, B–D, black columns) but differed markedly between elements, with F_{Mg} at 78%, F_{Ca} at 60%, and F_K as low as 30%. In eight of the 10 samples imaged after 20 min of tracer uptake, the largest potassium tracer fraction F_K was in vessel lumina, and in two samples (including that in Fig. 3), the tangential walls of the metaxylem bundles showed the largest fractions, by a small margin (Fig. 3C, right side). Vessel F_K was occasionally lower on the outer rims (Fig. 3C, green arrows), with larger fractions toward the center. In contrast, F_{Mg} and F_{Ca} values were quite homogeneous within the vessel lumina (Fig. 3, B and D).

The tracer fractions for the different elements showed strong differences among tissues, with the

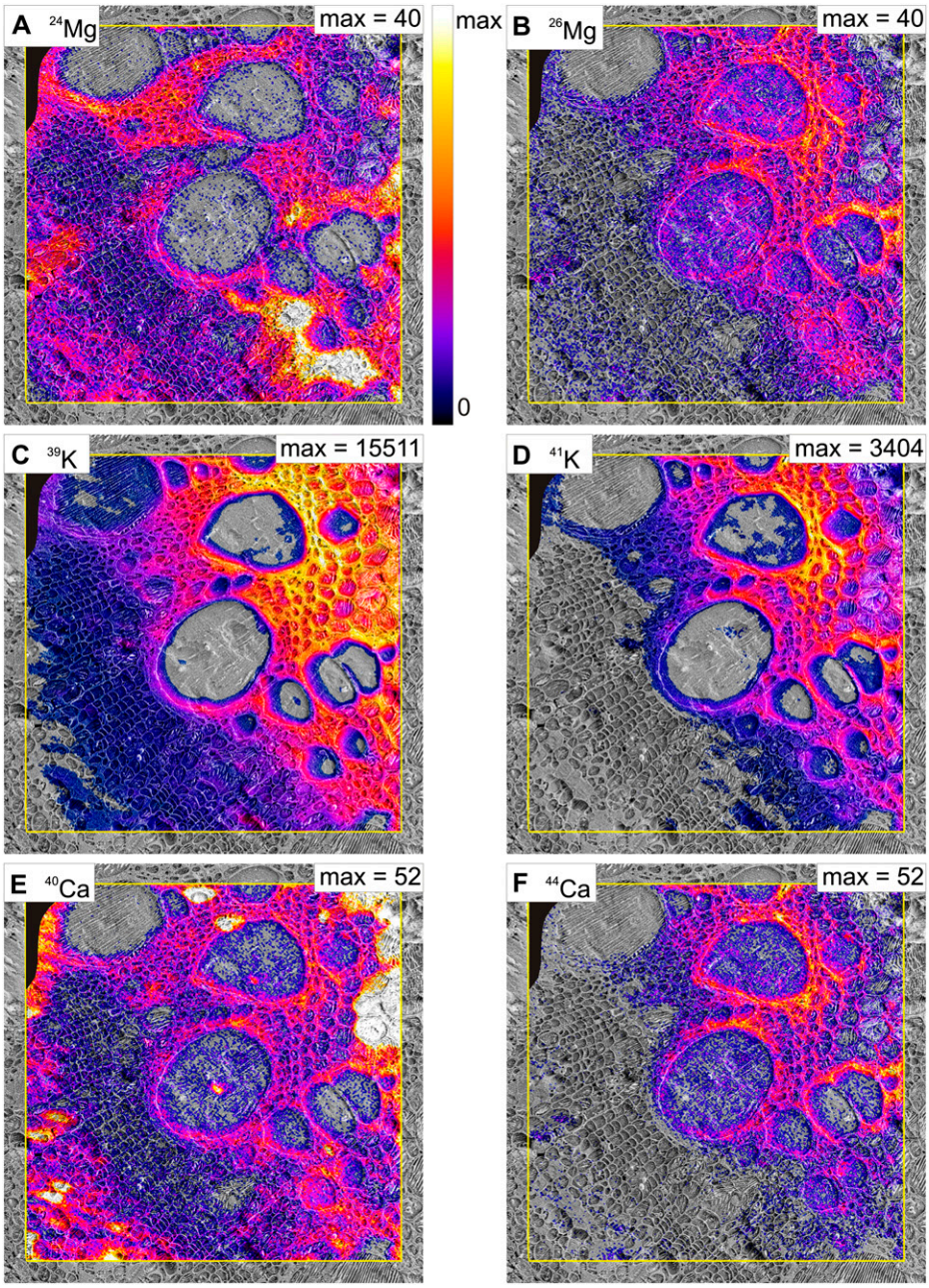

Figure 2. Cryo-SIMS mapping of signals of major isotopes of magnesium, potassium, and calcium. The images show the major natural isotope (left) and the major tracer isotope (right) in a sample taken after 20 min of continuous tracer application via the cut stem. The isotope images are laid over the corresponding cryo-SEM images (Fig. 1A). The yellow frame indicates area analyzed by cryo-SIMS. Scaling is linear from zero signal (S in counts per pixel) to individual maxima indicated in each image. In A and E, these were selected to optimize the display of detail in most parts of the images, at the expense of occasional oversaturation resulting in featureless white areas in the ^{24}Mg and ^{40}Ca images. Original maximum signal was for 96 (A) and 434 (E). For better visualization, pixels were set transparent where fractions fell below a threshold of the scale: 6% for A, B, E, and F and 3% for C and D. A small area in the top left corner of the images is blackened out and excluded from interpretation where the surface had not been properly cryo-planed. Area scanned by cryo-SIMS was 500 × 500 μm, 256 × 256 pixels.

largest fractions for all elements occurring in xylem parenchyma surrounding the vessels. F_{Mg}, for example, in the half-sheath facing the pith (XP-pi) was two-thirds of that in the vessels, in the parenchyma more distant from the vessels (XP-xv) was slightly lower, and in the half-sheath facing the cambium (XP-cm) reached only one-third of that in the vessels. Potassium showed a similar pattern, but calcium fractions, surprisingly, were identical in XP-pi and vessels and only slightly lower in the XP-cm and XP-xv (Fig. 4, B–D). Identical values to the vessels were found for F_{Ca} in the islands of thin-walled xylem parenchyma (XP-is) as well, whereas F_K and F_{Mg} were much lower in this tissue area than in the thick-walled xylem parenchyma. Other parts of the thin-walled xylem parenchyma (Fig. 1A, XP-th) between XP-cm and the cambium showed smaller fractions for all elements, which for calcium were still markedly higher than those of the cambium (Fig. 3D). The pith bordering the xylem parenchyma toward the center of the stem showed large magnesium fractions, F_{Mg} (almost one-third of vessel values; Fig. 4B), while potassium and calcium fractions were very low (Fig. 4, C and D).

Tracer fractions for all three elements in the cambium and phloem were much lower than for the neighboring XP-cm (Fig. 4, B–D). F_{Mg} was about half of the corresponding thick-walled xylem parenchyma values in both tissues, and F_{Ca} also was half the XP-cm

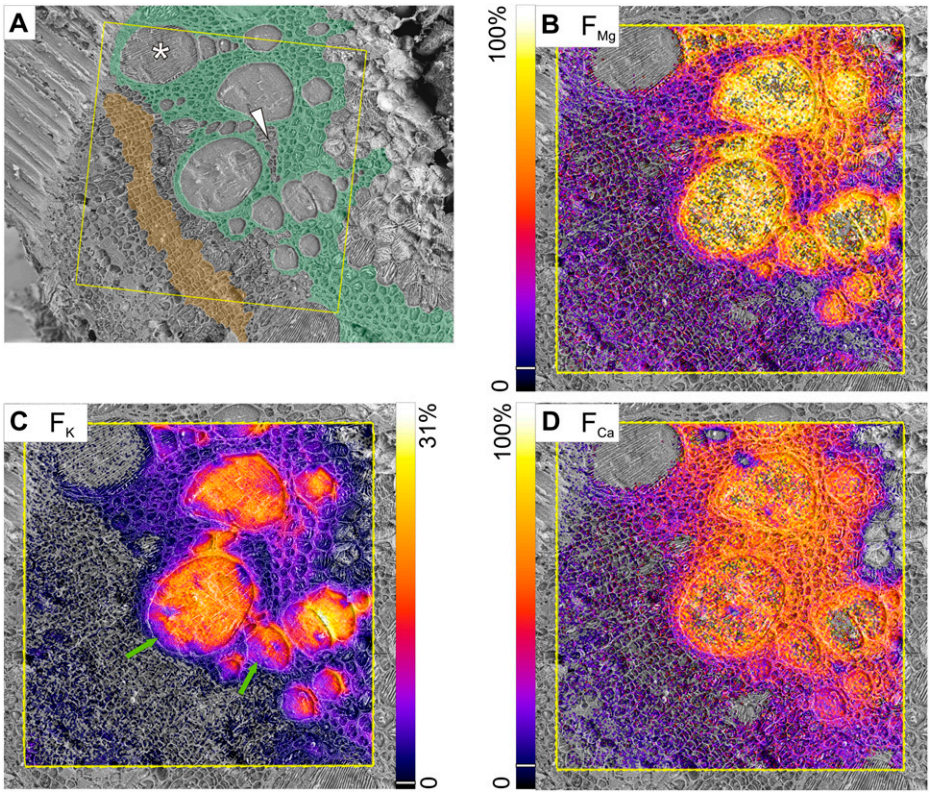

Figure 3. Mapping of fractions of magnesium, potassium, and calcium, originating from the tracer solution, from samples taken after 20 min of continuous tracer application via the cut stem. A, Cryo-SEM image with color-coded overlay to help in the identification of tissue types: thick-walled xylem parenchyma (green) and cambium (orange). The asterisk indicates an immature vessel, and the white arrowhead indicates an island of thin-walled xylem parenchyma within thick-walled parenchyma. B to D, Fractions of tracer (F_{Mg}, F_K, F_{Ca}) computed from cryo-SIMS isotope mapping are scaled from zero to the indicated maxima. For better visualization, pixels below the following threshold of the scale (indicated by white lines in the color bars) were set transparent: F_{Mg} and F_{Ca}, 6%; F_K, 2%. Area scanned by cryo-SIMS was 500 × 500 μm^2, 256 × 256 pixels. Images were overlaid on the corresponding cryo-SEM images. Green arrows indicate lower F_K values along the outer rim of two xylem vessels.

value in the cambium but lower in the phloem. F_K was below the detection limit (Fig. 4C).

Distributions of Potassium at High Spatial Resolution

More detail of the transport pathways was gained with cryo-SIMS in a mode giving higher spatial resolution (better than 1 μm), allowing us to differentiate between borders and lumina of individual cells (Metzner et al., 2008). The high spatial resolution mode, however, sacrifices mass resolution, so no useful images for magnesium and calcium tracers were possible (Metzner et al., 2008).

An area including metaxylem vessels, xylem parenchyma, and pith (Fig. 1A, next to V4) was chosen for high spatial resolution imaging to show more detail of movement toward the stem center (Fig. 5A). The largest vessel lumen had an F_K value of 20% (Fig. 5B), very close to the value in Figure 3C, where there was no uncertainty due to low mass resolution. The fractions in the cell walls of the thick-walled xylem parenchyma (XW) were half of this value (9%; Fig. 5B), with only 3% in the lumina of the thick-walled xylem parenchyma cells adjacent to the vessel (XL). Similar fractions were found for the cell walls of the pith (PW) and only 1% in the lumina of the pith cells (PL).

Transpiration Rate

When transpiration (and tracer uptake) rate was almost halved to 0.1 mL min^{-1} by increasing air humidity, tracer fractions of all three elements gave very similar images to those in Figure 3, B to D (data not shown), and the fractions of tracer for all three elements in most tissues were hardly affected (Fig. 4, B–D, white columns; $n = 3$). One possible effect was for magnesium and potassium in the XP-cm, where their tracer fractions were lower at the lower transpiration rate.

Xylem Tension during Tracer Application

Xylem tension in the intact plant, monitored by xylem pressure probe, was stable at 0.107 MPa relative to atmosphere (Fig. 6A). Cutting the stem under water caused a reduction to 0.02 MPa, an 81% loss of tension. In contrast, application of a nutrient solution via microcapillary led to a much smaller tension loss of 8% (measured by a separate xylem pressure probe; Fig. 6B, downward arrow). On subsequent withdrawal of the application capillary (Fig. 6B, upward arrow), tension returned to its initial value, confirming the pressure probe's precision and showing that the small measured tension loss was due to solution entry to the xylem. Further insertions and withdrawals of the application microcapillary yielded similar marginal tension drops and returns to original value (data not shown), emphasizing the minimally invasive character of the application approach. A total of six cut-stem applications and four capillary applications (Fig. 6C) showed a much more severe loss of tension with application by cut stem (81% ± 7%) than by capillary

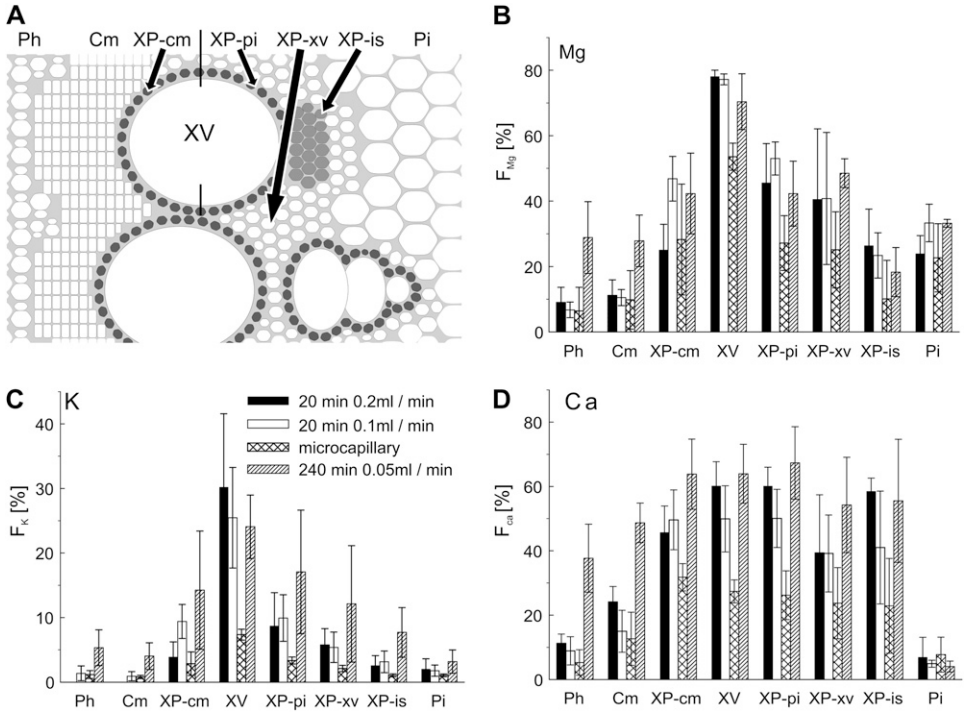

Figure 4. Fractions of tracer in various types of stem tissue. A, Scheme of the ROI, specified according to anatomical criteria defined in Figure 1. B to D, Fractions of magnesium, potassium, and calcium, originating from the tracer solution, for each ROI, from three different experiments (error bars indicating 1 SD). Black columns, 20-min cut-stem application, transpiration rate 0.2 mL min^{-1}. Fractions of potassium in the phloem and cambium were below the detection limit. White columns, transpiration rate 0.1 mL min^{-1}. Cross-hatched columns, microcapillary, 20-min application, transpiration rate 0.1 mL min^{-1}. Hatched columns, 240-min cut-stem application, transpiration rate 0.05 mL min^{-1}.

(11% ± 8%). This indicates that the pressure equilibrium between the xylem and the adjacent cells would be much more severely disturbed by cutting the stem; although the pressure-probed and injected vessels were not far apart, they were probably in separate bundles.

Tracer Distribution with Microcapillary Delivery

Solution inflow via microcapillary during the 20 min of application was 90 to 200 μL, a 450- to 1,000-fold replacement of xylem sap in a vessel (for a vessel diameter of 100 μm). This degree of replacement may be overestimated, because more than one vessel received some tracer (Fig. 7; two vessels), so the tracer solution may have moved into several vessels along the 2.5 cm between application and sampling sites. These sites were much closer and in the same internode, in contrast to the 25-cm separation in the cut-stem experiments. In preliminary experiments with a 25-cm separation, tracer delivered by capillary could not be detected, even in the xylem vessel lumina (data not shown), most likely due to dilution by natural element in the transpiration stream. Tracer fractions in the vessel lumina and in the tissues were smaller than those in cut stems (Fig. 4, B–D), but the distributions between tissues were similar (Figs. 3, B–D, and 7). Relative to the tracer fractions in xylem vessels, the fractions of all tracers were larger in the tissues compared with the cut-stem experiments at the same transpiration rate (Fig. 4, B–D, cross-hatched compared with white columns), but the SD values were exceptionally high. F_{Ca} was equal in xylem vessels and the whole xylem parenchyma, an even larger region than with cut-stem application.

Tracer Distribution after a 240-min Cut-Stem Delivery

Since there will be an approach toward a steady state during tracer application, we took samples after 240 min to compare with the 20-min samples. Transpiration rates in these experiments started at 0.12 mL min^{-1} and decreased with application time to values around 0.04 mL min^{-1}, so that total solution uptake was 12 mL, a 260-fold replacement of the xylem fluid within the stem segment. As with the 20-min application, some vessels were probably nonconducting and immature, since all tracer fractions were negligible (Figs. 8, B–D). The images for all three elements (Fig. 8, B–D) were qualitatively very similar at 240 and 20 min (Fig. 3, B–D) with the exception of F_{Ca}, which was much higher in the cambium and phloem after 240 min. Fractions in the vessels, xylem parenchyma, and pith at 240 and 20 min were very similar (Fig. 4, B–D, cross-hatched compared with black and white columns), while tracer fractions in the cambium and phloem were at least twice as large after 240 min of tracer application than after 20 min.

High lateral resolution images of F_K from metaxylem areas were acquired for 240-min as well as for 20-min samples (Fig. 9A). F_K in the vessel lumen (XV; 20%; Fig. 9B) was close to the overview image value (26%; Fig. 8C) and identical to the fraction at high lateral resolution in the 20-min sample (Fig. 5B). Fractions in surrounding tissues were mostly much larger at 240 min (Fig. 9B), even though data from overview

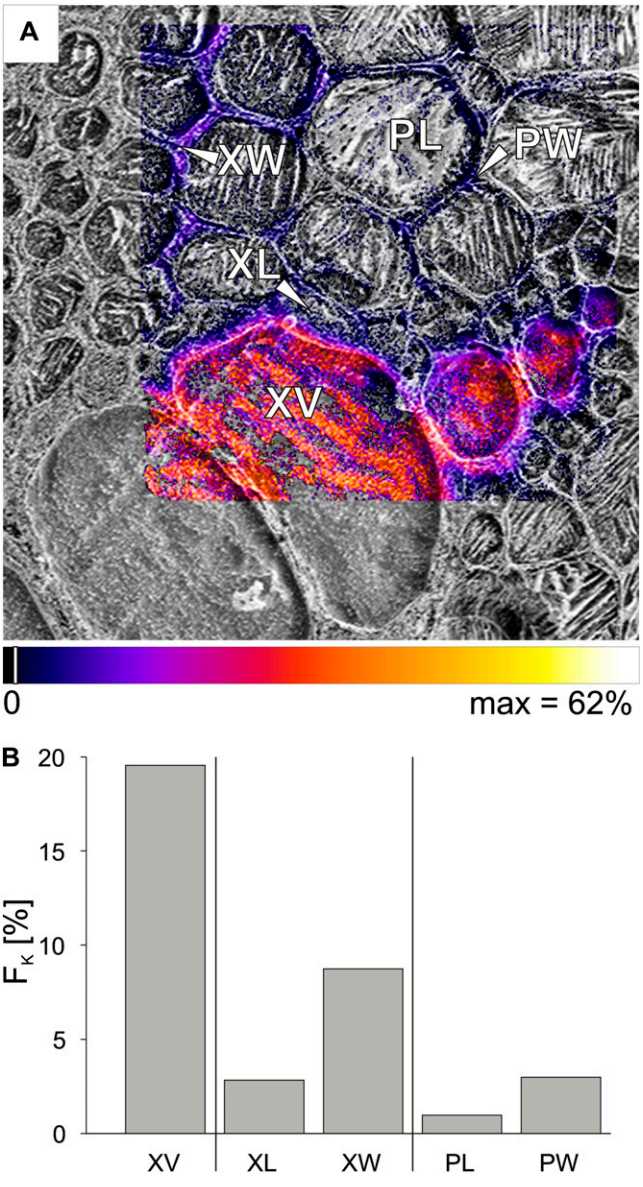

Figure 5. Mapping of fractions F_K of potassium, originating from the tracer solution, imaged at high spatial resolution after 20 min of tracer application via the cut stem. A, Potassium tracer fraction (F_K) imaged for a bundle of metaxylem vessels as overlaid on the corresponding cryo-SEM image. The area was also imaged at low spatial resolution, as shown on the right side in Figure 3C. B, Bar chart of F_K representing ROI for the xylem vessel (XV), the lumina (XL), and walls (XW) of small thick-walled xylem parenchyma cells bordering the vessel, as indicated in A. F_K was also calculated separately for the lumina (PL) and walls (PW) of the pith, as visible toward the top right in A. Area scanned by cryo-SIMS was 121 × 121 μm, 256 × 256 pixels. Pixels were set transparent for fractions below a threshold of 2% of the scale (indicated by white lines in the color bar). The striped appearance of the xylem vessel lumina is probably due to the growth of ice crystals (Metzner et al., 2008).

images showed an increase for the xylem parenchyma but none for the pith (Fig. 3C). This increase was not uniform; for example, cell lumina of the thick-walled xylem parenchyma (XL) were five times larger in 240-min than in 20-min samples but still below the fractions in the cell walls (XW). In the pith, fractions in both cell walls and lumina increased 3-fold from 20 to 240 min.

DISCUSSION

We utilized stable isotope tracers of magnesium, potassium, and calcium to characterize the exchange of these mineral nutrients between the transpiration stream and surrounding stem tissues, measuring all isotopes in frozen hydrated stem samples by cryo-SIMS (Metzner et al., 2008). In samples taken 25 cm above a cut where tracer solution entered the transpiration stream continuously for 20 min, all tracers were detectable in the xylem vessels and strong radial spreading into surrounding tissues had occurred.

An important issue for interpreting our data about radial movement of the nutrients was the possible influence of radial water movement. Cutting the shoot under water may have caused an artifact, since the dramatic release of xylem tension and the drop in osmolality would have resulted in transient flows of water into adjacent tissues in relation to their different elastic moduli. If this flow carried xylem nutrients (solvent drag), the tracer could also have moved, and our data would not reflect an intact system. However, when tracers were applied via microcapillary, which was shown to hardly affect xylem tension, the radial movement of tracer into tissues was, if anything, larger (Fig. 4, B–D), the opposite of the proposed effect. This is a good basis for supposing that a transient flow did not cause artifacts. It was unexpected, because the time scale for reestablishment of osmotic and hydrostatic gradients, and therefore the expected water and solute redistribution, in root cortical cell layers after cutting apices or side roots can be quite long (10–30 min; Zimmermann et al., 1992; Rygol et al., 1993). It may be that the transient had expired before tracer arrived at the sampling site, 25 cm from the cut. The time for solution to arrive would have been only about 30 s, but it is possible that significant amounts of tracer did not arrive at the sampling site by then, due to radial loss of tracer from the xylem vessels all along the intervening path (see below). Our findings, however, are consistent with the results of Wegner and Zimmermann (2009), where radial potassium transport into maize (*Zea mays*) roots had little, if any, dependence on xylem pressure. A possible explanation for this discrepancy is that potassium, although generally considered to be an important osmoticum, together with magnesium does not play a major role in establishing radial osmotic gradients.

Taken together, our data strongly suggest that the predominant mechanism for movement from xylem into adjacent tissues was via diffusion; therefore, the distribution of solutes is probably determined more by the parameters affecting their diffusion, such as charge and polarity, than by movement with water. There was no evidence of nutrient movement with water from the comparison of tracer distributions after the cut-stem or

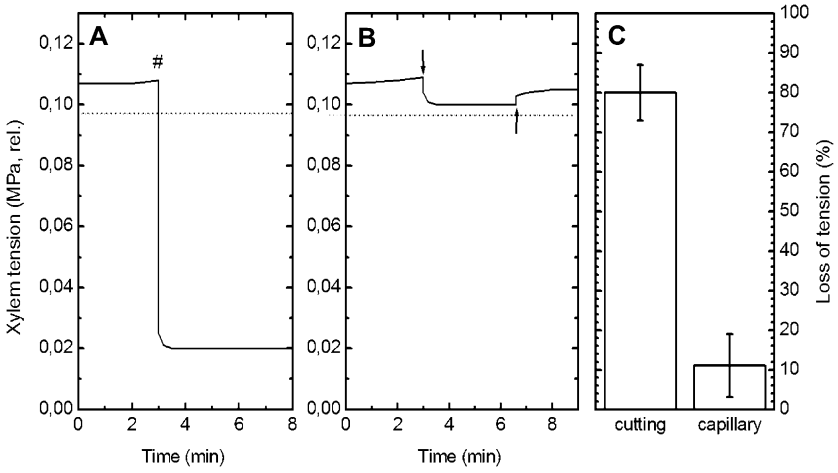

Figure 6. Xylem tension (relative to the atmosphere) monitored by the xylem pressure probe during experiments parallel to tracer applications. A, Application via the cut stem. The number sign (#) indicates cutting of the stem under water. B, Application via a microcapillary. The downward arrow indicates insertion of the application microcapillary, and the upward arrow indicates withdrawal of this microcapillary. The horizontal dashed lines in A and B mark the saturation water vapor pressure (0.0977 MPa). C, Percentage loss in tension via the cut stem ($n = 6$; mean ± SD) and with capillary application ($n = 4$).

capillary application. Also, when the transpiration rate was decreased 2-fold, there was very little change in the radial distribution patterns of the nutrient tracers (Fig. 4, B–D), even though hydrostatic and osmotic pressure profiles in different herbaceous species can be affected by transpiration rates (Rygol et al., 1993; Wistuba et al., 2000). Only F_{Mg} in the xylem parenchyma toward the cambium was lower at higher transpiration rates, consistent with an inverse relationship between tracer spreading and the axial flow rate found by van Bel (1974) for the radial escape of amino acids from the xylem of tomato (*Solanum lycopersicum*). Due to this relationship, we cannot exclude movement by nondiffusive processes like solvent drag for this tissue area.

Tracer Movement in the Xylem Vessels

The tracer fractions remaining in the vessels at the sampling site reflect the interactions between transpiration stream and stem tissues all along the xylem pathway from the solution. This fraction of all three element tracers was significantly below that of the applied tracer solution, even after longer feeding

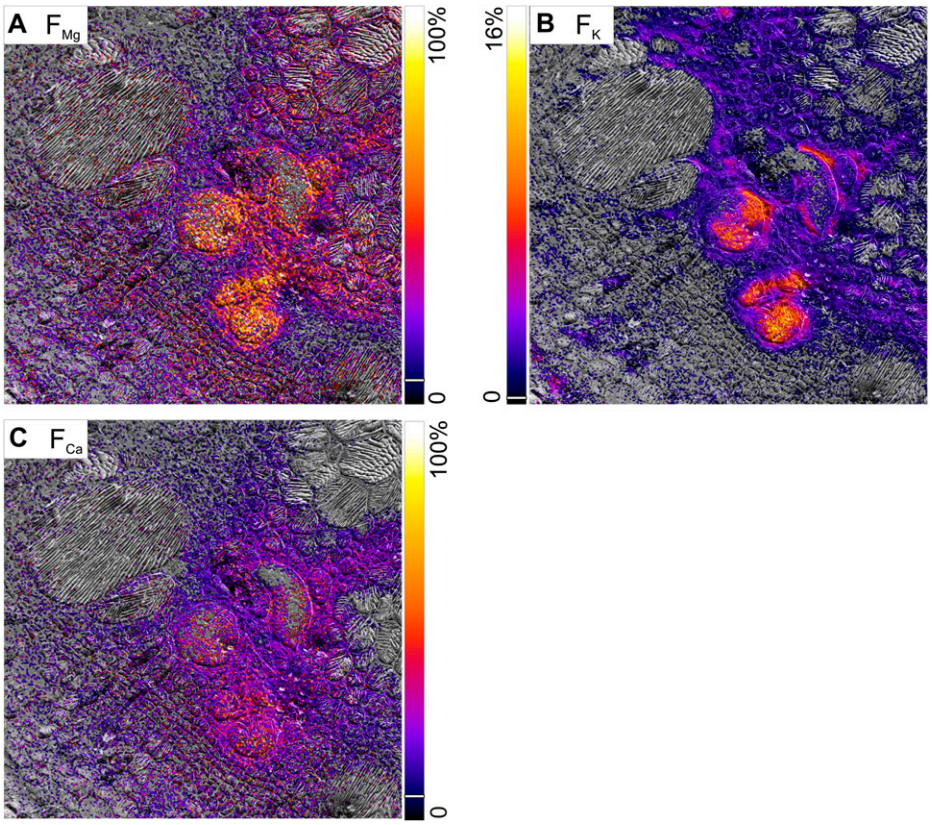

Figure 7. Microcapillary application. Mapping of fractions of magnesium, potassium, and calcium, originating from the tracer solution, for samples taken after continuous tracer application for 20 min. The images are overlaid onto the corresponding cryo-SEM images. Area scanned by cryo-SIMS was 500 × 500 μm, 256 × 256 pixels. For better visualization, pixels below the following thresholds of the scale (indicated by white lines in the color bars) were set transparent: F_{Mg} and F_{Ca}, 6%; F_K, 2%.

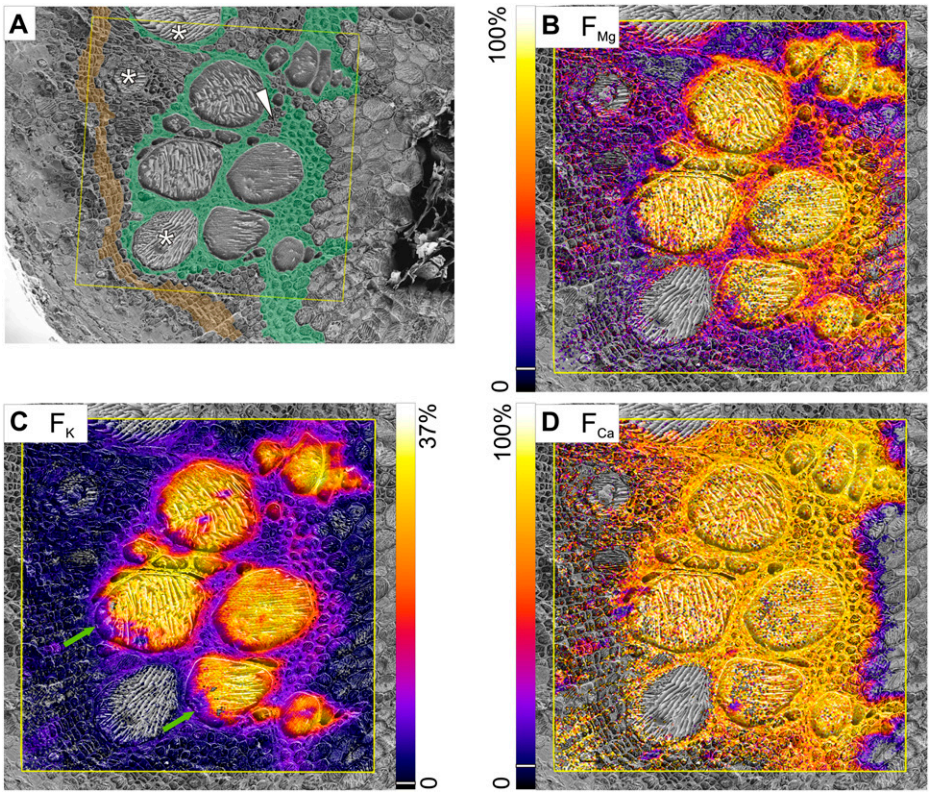

Figure 8. Mapping of fractions of magnesium, potassium, and calcium, originating from the tracer solution, in samples taken after 240 min of continuous tracer application via the cut stem. A, Cryo-SEM image with color-coded overlay to show tissue types: thick-walled xylem parenchyma (green) and cambium (orange). Asterisks indicate immature vessels, and the white arrowhead indicates thin-walled xylem parenchyma within thick-walled parenchyma. B to D, Fractions of tracer (F_{Mg}, F_K, F_{Ca}) are scaled from zero to the indicated maxima. For better visualization, pixels below the following thresholds of the scale (indicated by white lines in the color bars) were set transparent: F_{Mg} and F_{Ca}, 6%; F_K, 2%. Area scanned by cryo-SIMS was 500 × 500 μm^2, 256 × 256 pixels.

periods, and the most likely reason for these low fractions is the isotopic dilution of tracer by a significant influx of solutes to the xylem, at natural isotopic abundance, from surrounding tissues along the 25-cm pathway from the point of tracer entry. Because xylem vessel isotope fractions did not change very much with time (from 20 to 240 min), we can conclude that the material entered the xylem with both rate and isotopic composition unchanging, suggesting that it came from a pool that was either not accessible for nutrients from the vessels or so large that its isotopic composition did not change significantly. This inflow of element with natural isotopic abundance differed strongly between the studied elements (the fraction originating from the tracer solution was reduced to 80% for magnesium, 60% for calcium, and 30% for potassium; Fig. 4, B–D). Because the concentration of each element supplied in the tracer solution was the same, we can infer that the element fluxes into the vessels were smallest for magnesium and largest for potassium, apparently the more available cation. The lower fractions of potassium tracer at the rim of larger vessels compared with the center (Figs. 3C and 8C) are consistent with a potassium influx from surrounding tissue, perhaps replenished from the phloem (Lang, 1983).

Tracer Flows from the Xylem Vessels to the Surrounding Tissues

Radial spreading of all tracers was dependent on element and tissue structure rather than on distances from the xylem vessels, the source of tracer. The large gradients in tracer fractions between xylem vessels and the different stem tissues confirm the successful immobilization and imaging of the diffusible cations by our protocols.

Xylem Parenchyma, Thick Walled

The thick-walled xylem parenchyma, in direct contact with the xylem vessels, showed the strongest labeling of all tissues for all three elements. Within the xylem parenchyma, the fractions (F) in the cells enclosing the conducting xylem vessels (XP-pi and XP-cm) generally were only slightly larger than those in the more distant XP-xv, suggesting intense nutrient exchange within this thick-walled tissue. This is in contrast to the xylem parenchyma in trees, where there is a functional difference between cells of the axial sheath of the xylem vessels and those in the bulk of the xylem parenchyma concerning exchange of solutes with the vessels occurs (van Bel, 1990), and indicates that the whole xylem parenchyma contributes equally to the exchange of mineral nutrients with the xylem vessels.

The fractions (F) of both magnesium and potassium were well below those in the vessels, and they were very similar at 20 and 240 min and thus probably in a steady state by 20 min (Fig. 4, B and C). The exchangeable fractions in the xylem parenchyma were nowhere near 100% (60% for Mg and 30% for potassium; see Eq. 4), indicating that very significant quantities of both

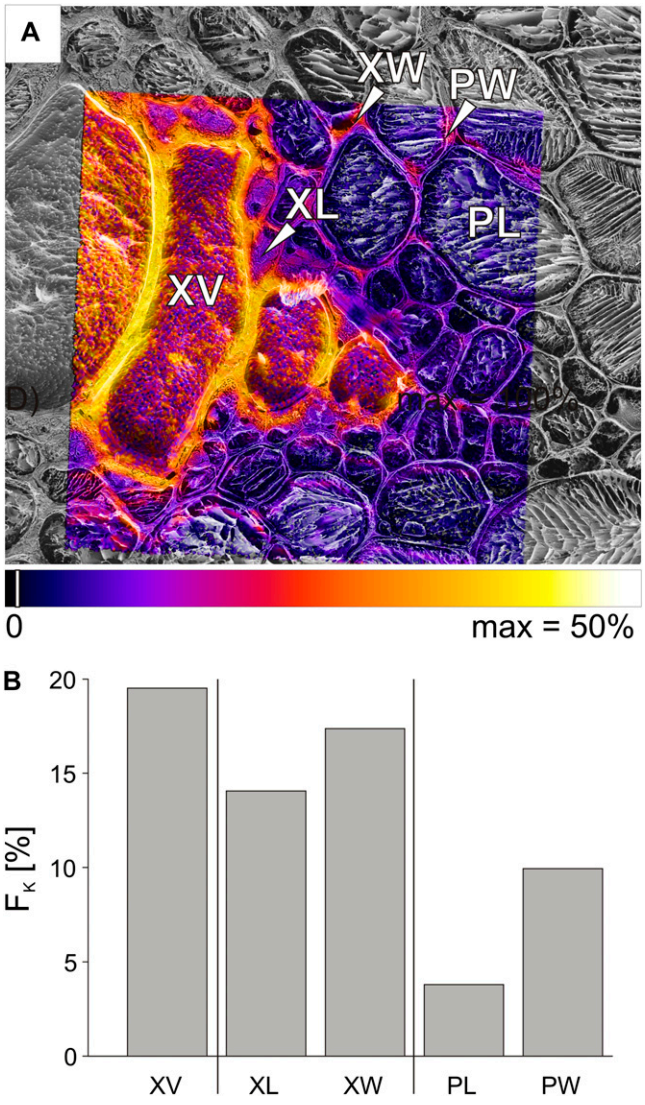

Figure 9. Mapping of the fraction of potassium, originating from the tracer solution, imaged at high spatial lateral resolution after 240 min of continuous tracer application. A, Potassium tracer fraction (F_K) overlaid on the corresponding cryo-SEM image imaged for a bundle of metaxylem vessels (same as in top right corner in Fig. 8C). B, Bar chart of F_K for the xylem vessel (XV), the lumina (XL), and walls (XW) of small thick-walled xylem parenchyma cells bordering the vessel as indicated in A. F_K was also calculated separately for the lumina (PL) and walls (PW) of the pith, as visible toward the top right in A. Area scanned by cryo-SIMS was 115 × 115 μm^2, 256 × 256 pixels. Pixels were set transparent for fractions below a threshold of 2% of the scale (indicated by the white line in the color bar).

nutrients in this tissue were not exchangeable with nutrients from the xylem. Presumably, they are physically isolated (e.g. enclosed in vacuoles) or chemically bound (e.g. magnesium in Mg-ATP or phosphate and calcium in pectins).

Since potassium is not likely to be bound in plant tissues (Marschner, 1995), its nonexchanging fraction is likely to be vacuolar, and indeed the cell lumina F_K was low (Fig. 5). Symplastic potassium exchanged more slowly than the apoplast with the xylem vessels, so that after 240 min, the tracer fractions were higher and the difference between apoplast and symplast was reduced (Fig. 9B). Nevertheless, a symplastic tracer fraction was detectable by 20 min, even though a normally high symplastic concentration (Leigh, 2001) would dilute the tracer. This suggests a fast potassium turnover there, maybe a sign of the transmembrane fluxes associated with the regulation of turgor and concentration (Szczerba et al., 2006).

Potassium tracer in the apoplast of the xylem parenchyma clearly took an apoplastic route from the xylem vessels, since the tracer fractions along the symplastic route (of the thick-walled xylem parenchyma) were lower than at the destination. F_E at the destination can never exceed F_E in the source of tracer, in contrast to concentrations (due to membrane processes), since isotopic abundance and F_E could only increase by selective enrichment of a single isotope. Such isotope effects do occur in plants (e.g. for magnesium; Black et al., 2008), but they are minuscule.

The distribution of F_{Ca} in this tissue was quite unlike magnesium and potassium, being equal to xylem vessel lumina after 20 min (Fig. 4D), indicating that all calcium was exchangeable and not bound or located behind a significant diffusion barrier. This high exchangeable fraction is surprising, as, in sugar beet (*Beta vulgaris*), more than three-quarters of the calcium is firmly bound to pectates in the cell walls and as phosphates (Marschner, 1995). Furthermore, this shows that calcium is more mobile than potassium and magnesium in this tissue, which is quite puzzling, since the mobility of monovalent ions in tissues is usually higher than that of divalent ions. It may be that magnesium and potassium were mostly in the symplast behind membranes, while the largest amounts of calcium were in the apoplast, where they could exchange with the xylem vessels. Any significant amount of symplastic calcium would be at high-affinity, but very accessible, binding sites, with high futile cycling and rapid regulation of calcium.

The conclusion, therefore, is that all these xylem nutrients exchanged quickly with the thick-walled xylem parenchyma. It also showed a particularly high signal of the natural isotopes of magnesium and potassium (Fig. 2, A and C), suggesting that they had high concentrations in this tissue (remembering, however, that signal images are subject to matrix artifacts). If so, the large exchanged fractions show that there was massive exchange of nutrients with the xylem parenchyma, consistent with its commonly perceived role as a reservoir for xylem-tissue exchange (van Bel, 1990). This interpretation fits well with van Bel (1978) and Wolterbeek et al. (1985), finding a large and rapidly exchanging (<15 min) apparent free space of the xylem in tomato. Nevertheless, our results suggest that the symplast can also provide this fast exchange.

Xylem Parenchyma, Thin Walled

Like the thick-walled xylem parenchyma, the "islands" of thin-walled xylem parenchyma reached a steady state by 20 min, with similar fractions as in the thick-walled xylem parenchyma, except F_{Mg}, which was notably lower than in the surrounding parenchyma (Fig. 4B). This low fraction may reflect a large amount of stored magnesium, since the signal of the major natural magnesium isotope was high (Fig. 2A), so these thin-walled parenchyma islands may have a magnesium storage role, corresponding to the endodermis of spruce (*Picea abies*) needles found by Stelzer et al. (1990).

Pith

The pith was clearly much less accessible for xylem nutrients than the xylem parenchyma. Tracer fractions for potassium and calcium were very low (3% and 5%), even after 240 min, and only about 10% of these nutrients in the pith was exchangeable. These low exchangeable fractions probably reflect large amounts of potassium and calcium (e.g. in vacuoles), with the pith being a storage tissue for nutrients (van der Schoot and van Bel, 1990; Koroleva et al., 2000). Indeed, the signal for the natural isotopes of potassium and calcium was high in the pith (Fig. 2, C and E), suggesting that their concentrations were high. In contrast, pith magnesium fractions were almost as large as in the xylem parenchyma, indicating that there was no blockage of magnesium (and possibly other nutrient) movement between the xylem vessels and the pith. The pathway for nutrient movement between the xylem vessels and the pith is most likely apoplastic, since there were much larger fractions of potassium in the cell walls of both the xylem parenchyma and the pith compared with the cell lumina (Fig. 5B). This pathway has been suggested for tomato (van der Schoot and van Bel, 1990), because both dye movement and electric coupling between cells showed that the pith symplast was isolated from the xylem parenchyma.

Cambium and Phloem

There were very low tracer fractions in cambium and phloem for all three nutrients, but no steady state had been reached at 20 min, since the fractions had increased significantly at 240 min. The low values after 20 min are striking, since the cambium is very close to the vessels, separated by only one or two cell layers of xylem parenchyma, where tracer fractions were high for all nutrients. For calcium, the large values of F_{Ca} at 240 min suggest that the fraction may be as large as in the thick-walled xylem parenchyma at steady state, with an exchangeable fraction of 100%. Therefore, the small fractions at 20 min suggest a slow cation-exchange rate between the xylem vessels and the cambium. The discontinuity in potassium and magnesium, with fractions in cambium and phloem almost equal but much lower than in the neighboring xylem parenchyma, is most likely caused by the barrier at the interface between xylem parenchyma and cambium. It may be a diffusion barrier, a large but particularly slowly exchangeable fraction in the cambium/phloem, or a combination of both. Such an apoplastic barrier would also help to prevent sugar and other solutes in the phloem apoplast from escaping into the xylem (Minchin and Thorpe, 1984). A similar situation was reported for cation uptake from a hydroponic tracer solution, showing a tracer discontinuity at the root endodermal barrier, with almost identical fractions to those we saw, after the same time of application (Kuhn et al., 2000).

CONCLUSION

For nutrient distribution within plants, these findings have several implications. There is an intense exchange between xylem vessels and the surrounding tissues that contain accessible reservoirs of various sizes and exchange properties for the regulation of nutrient fluxes in the xylem. Rapid exchange with the thick-walled xylem parenchyma enlarges the storage volume and capacity of the xylem translocation pathway and provides short-term buffering of fluctuations in xylem sap concentration for all three nutrients, including calcium. A slower exchange, but with a larger nutrient pool, is provided by the pith, cambium, and phloem. Of these, the phloem is also the route for many nutrients to be exchanged with other parts of the plant (Marschner et al., 1997; Jeschke and Hartung, 2000), for coordinating the delivery of ions according to the needs of tissues and organs, and to avoid their delivery to organs where excess concentrations could be harmful. But because calcium is hardly mobile in phloem, it appears that its storage is purely local, with fast access in the xylem parenchyma and long-term storage in the pith.

Table II. *Environmental conditions for growth and during experiments*

In cut-stem tracer application experiments (1, 2, 4), tracer uptake rates were indistinguishable from the transpiration rate of uncut control plants under the same environmental conditions. In capillary application experiments (3), transpiration rate was 0.1 mL min^{-1}. In 240-min experiments (4), uptake rates began at 0.1 mL min^{-1} and were below 0.05 mL min^{-1} after 20 min.

Experiment	Sampling Time	Application	Relative Humidity	Tracer Uptake Rate
	min		*%*	*mL min^{-1}*
1	20	Cut stem	35	0.2
2	20	Cut stem	66	0.1
3	20	Microcapillary	40–70	0.001
4	240	Cut stem	44–63	<0.05

MATERIALS AND METHODS

Plant Material

Plants of French bean (*Phaseolus vulgaris* 'Fardenlosa Shiny') were grown from seeds in 1.7-L pots with standard soil substrate (ED 73; Einheitserde) in a growth chamber with a 12-h/12-h light/dark cycle, illumination of 300 μmol m^{-2} s^{-1} (photosynthetically active radiation) with fluorescent lamps (15 × 36-W Fluora; Osram), temperature between 21°C and 23°C, and automatic watering twice a day. Plants approximately 4 weeks old were used for experiments, when they had about three mature trifoliate leaves. Transpiration rate was measured under the same environmental conditions as for tracer experiments by measuring weight loss, with pots wrapped in plastic to prevent evaporation.

Collection of Xylem Sap

Epicotyl and first internode above the primary leaves were excised and cut into pieces approximately 5 cm long. These were placed upright in 15-mL centrifugation tubes on a polytetrafluoroethylene sieve, and the tubes were closed and centrifuged for 5 min with 1,560*g*. The volumes of the collected sap were determined by weighing. The osmolality of the xylem sap was determined by a freezing point osmometer (Micro-Osmometer model 210; Fiske Associates) to be 48 ± 13 mosmol kg^{-1} (n = 5).

Tracer Application

The multielement tracer solution contained 2.5 mM $^{26}MgCl_2$, ^{41}KCl, $^{44}CaCl_2$, and $NaNO_3$ (Sigma-Aldrich) in deionized water. $^{26}MgCl_2$ and $^{44}CaCl_2$ were purchased from Medgenix. ^{41}KCl for 20-min experiments at low transpiration was obtained from Isoflex. For the other experiments, ^{41}KCl was purchased from Medgenix. The isotopic enrichment of the tracers is shown in Table I. Solution osmolality was 24 mosmol kg^{-1}.

We used two protocols to supply tracer to the transpiration stream. For cut-stem applications (experiments 1, 2, and 4 in Table II), the bean shoot was cut under tap water (6 mosmol kg^{-1}) directly above soil, and the wet end was rapidly transferred into the tracer solution, which was then taken up by the transpiration stream for 20 or 240 min. For minimally invasive application (experiment 3 in Table II), the tracer solution entered the xylem in the first internode above the primary leaves via a glass microcapillary (1.0 and 0.6 mm o.d. and i.d., maximum outer tip diameter approximately 20 μm) attached to Tygon tubing (0.8 mm i.d.). A micromanipulator slowly moved the capillary tip radially into the shoot tissue while observing the meniscus, formed within the tubing by the tracer solution, continuously with a microscope. Forward movement of the tip was immediately stopped when the meniscus moved suddenly toward the plant. The tubing was chosen long enough that the meniscus did not reach the tip of the capillary during application. This microcapillary application extended for 20 min only. Environmental conditions during both protocols are displayed in Table II.

Pressure Probe

Xylem pressure probe measurements (Benkert et al., 1991) used parallel experiments with tracer-free solutions. Experimental conditions were 5 to 20 μmol m^{-2} s^{-1} photosynthetically active radiation, 20°C to 25°C, and 47% to 70% relative humidity, more variable than for the tracer application experiments. After inserting the xylem pressure probe into the xylem of the first stem internode and reading a reasonably constant xylem tension for several minutes, one of the two solution application protocols was undertaken while measuring the tension. Although the application capillary was positioned as close as possible to the tip of the pressure probe, it is most likely that both capillaries were inserted in different xylem vessels. However, since neighboring xylem vessels of the same organ are tightly hydraulically coupled (Benkert et al., 1991; Thürmer et al., 1999; Wistuba et al., 2000; Schneider et al., 2007), pressure changes caused by solution application should be detectable with the pressure probe in the other vessel. When the tension dropped to 0.0977 MPa relative to atmosphere (corresponding to water vapor pressure at room temperature), it was provoked to rise above that critical value to demonstrate a firm hydraulic coupling all the way from xylem to pressure sensor (absence of water vapor or air bubbles); otherwise, the measurement would be invalid.

Preparation of Frozen-Hydrated Tissue Samples

Frozen-hydrated tissue samples were prepared according to Metzner et al. (2008). Briefly, approximately 4-cm-long pieces from the first internode above the primary leaves were excised for the cut-stem tracer application experiments, their mid-section being 25 cm above the application site and for microcapillry application 2.5 cm above the application site. The samples were mounted in copper rivets by the aid of a Suc solution and shock frozen by plunging into melting propane (−189°C), all within 30 s after excision. During subsequent preparation and measurement, the sample temperature was continuously kept below −130°C. Frozen samples were trimmed and their surfaces planed prior to the cryo-SIMS analysis with the aid of a cryo-microtome (MED 020/GBE with BU 012092-T and VCT-100; BAL-TEC). The samples were subsequently transferred via the VCT-100 cryo-shuttle through the respective airlock systems to the cryo-SIMS and the cryo-SEM systems.

Cryo-SIMS Measurements

Isotope mapping on the cryo-planed frozen-hydrated bean stem samples was performed with a ToF-SIMS IV time of flight secondary ion mass spectrometer (IONTOF) equipped with an airlock system, a modified cryo-stage, and a presputtering O_2^+ ion beam with 2 keV as described in detail by Metzner et al. (2008). A mass-filtered 25-keV pulsed Bi^+ or Bi^{3+} ion beam was used for generation of the secondary ions. The ion beam current was between 0.1 and 1.2 pA, resulting in a primary ion dose density between 1.3×10^{13} and 6.9×10^{13} ions cm^{-2}. To prevent charging of the sample surface, a low-energy electron flood gun was used. A complete secondary ion mass spectrum was recorded for each pulse and pixel.

Two types of measurements were conducted during the 6- to 8-h measuring time for the same sample. (1) Overview images were acquired with the high-current bunched mode with Bi^+ (Figs. 2 and 3, B–D) or the low-current bunched mode with Bi^{3+} (Figs. 7 and 8, B–D), yielding large area views (500 × 500 μm^2) with high secondary ion yields per primary ion pulse at high mass resolution ($m/\Delta m$ = 3,500 at mass 41) and spatial resolution of 10 to 7 μm. (2) For high spatial resolution images (Figs. 5 and 9), the burst-align mode with Bi^+ or Bi^{3+} gave ion maps of small tissue areas (<150 × 150 μm^2) at a spatial resolution better than 1 μm but with lower secondary ion yields per primary ion pulse and nominal mass resolution. At nominal mass resolution, other secondary ions interfered with the detection of the isotopes of interest, and data from this measurement type were suitable only for the potassium isotopes. ^{39}K gave a high enough signal for mass interferences to be negligible, but at nominal mass 41, up to 20% of the signal originated from carbohydrates (as seen at high mass resolution; Metzner et al., 2008). Therefore, at high spatial resolution, there would be unresolvable signal from these ions along with ^{41}K, particularly in areas with high organic content. For calcium and magnesium isotopes, however, signal from the interfering ions seen at high mass resolution were too high for the images to be meaningful at high spatial resolution.

Processing of Cryo-SIMS Data

Images of the major isotopes of the analytes were computed from the recorded mass spectra as ion counts per pixel. A "Poisson correction" (Stephan et al., 1994) was used because multiple events would sometimes have occurred within the detection interval. We denote the resulting value signal (S) in counts per pixel. In order to know the fraction of an element in each pixel that originated from the tracer solution, it is necessary to correct for the tracer isotope originally present in the plant tissue. Therefore, we calculated F_E, the fraction of element E originating from the tracer solution, from the abundance of the tracer isotope in the pixel (A_E) in relation to the tracer isotope abundance of the nutrient solution (A_{nE}), but in each case correcting for the natural abundance of the tracer isotope (A_{0E}). Being a fraction, F_E is not affected by topography or the chemical matrix of the sample.

$$F_E = \frac{A_E - A_{0E}}{A_{nE} - A_{0E}} \quad (1)$$

The natural abundance of the tracer isotope A_{0E} was taken from the literature (Böhlke et al., 2005), and the tracer abundance was calculated from the SIMS signals as:

$$A_E = \left(\frac{S^T}{\sum_I S^I} \right)_E \quad (2)$$

where S^I is the pixel signal of each isotope I of the element, and I = T for the enriched tracer isotope representing the element. A threshold was chosen for $\sum S^I$ below which we set $F_E = 0$ in order to mask noise. The chosen threshold was 1% of the image maximum for potassium and calcium and 5% for magnesium. Images of F_E were then scaled from zero to 255 and displayed in the NIH ImageJ "fire" palette. For individual tissues and tissue areas (Fig. 4, B–D), A_E was calculated by first defining ROI with the aid of the software IonImage (IONTOF) based on the anatomical information from the corresponding cryo-SEM images. For these regions, the sum of S^I over all pixels in the ROI was used for calculation of A_E (Eq. 2), and F_E was calculated according to Equation 1.

The Exchangeable Fraction of Element in the Tissues

After a steady state for isotopic exchange of an element (E) between the xylem sap and tissue is reached, the tracer of exchangeable (unbound) element will have equal abundance in each place but the nonexchangeable material will remain at natural abundance. Thus, if ions in the xylem sap are all unbound, with abundance A_{xE}, but the exchangeable fraction of the element in the tissue is e_{tE}, due either to chemical or physical sequestration, then the tracer abundance for the tissue (A_{tE}) is

$$A_{tE} = e_{tE}A_{xE} + (1 - e_{tE})A_{0E} \quad (3)$$

and from Equation 1:

$$e_{tE} = F_{tE}/F_{xE} \quad (4)$$

Limits of Detection for Stable Isotope Tracers with Cryo-SIMS

The detection limits for the stable isotope tracers depend on the precision and SD of the isotopic abundance measurements. To determine this limitation for our instrumental setup, we analyzed three air-dried spots of half-strength Hoagland solution with natural isotopic abundance on clean silicon substrate (Table I). Taking the error margins from Table I, it can be seen that ^{26}Mg can be detected under these conditions if its abundance exceeds the natural abundance by about 2.4%, likewise ^{41}K tracer by 1.0% and ^{44}Ca tracer by 0.2%. Of course, detection sensitivity depends on statistical variability where tracer counts are small, which is more likely for data from single pixels.

Cryo-SEM

The surfaces of frozen-hydrated samples were imaged with a LEO Gemini VP 1550 scanning electron microscope (Zeiss) with a cold-field emission electron source. The instrument is equipped with a BAL-TEC cryo-stage and an airlock for the cryo-shuttle. The samples were imaged at an acceleration voltage of 1.8 keV at a stage temperature below −120°C and a pressure of 2×10^{-3} Pa. The surface was etched by transiently raising the temperature of the sample stage to −90°C while the extent of sublimation was monitored by continuous scanning of the sample surface. Sufficient etching typically required 2 to 5 min. SEM images were optimized for printing using levels and curve settings in Adobe Photoshop.

Overlays of Cryo-SIMS Images onto Cryo-SEM Images

Ion and fraction maps are presented as overlays onto corresponding cryo-SEM images using Adobe Photoshop. Areas in the SIMS images with very low signal or tracer fractions were colored transparent, thus revealing the SEM structure, with lower inclusion threshold for magnesium and calcium isotope images (Fig. 2, A, B, E, and F) and for F_{Mg} and F_{Ca} images (Figs. 3, B and D, and 8, B and D) set to 6% of the full scale. The threshold for potassium isotope images (Fig. 2, C and D) was set to 3% and for F_K (Figs. 3C, 5A, 8C, and 9A) to 2% due to the very high signal (S^I) and low background in potassium. Since expected SD values for magnesium and calcium images were larger than the selected thresholds, no loss of relevant information arose from this procedure.

Supplemental Data

The following materials are available in the online version of this article.

Supplemental Figure S1. Supplemental Figure S1 shows the setup for the application of tracer by the cut-stem.

ACKNOWLEDGMENTS

We are very grateful to Alexandra Ley for performing light microscopy and some of the minimally invasive pressure probe and tracer application experiments. Marion Roeb and Anne Dreißen helped with plant cultivation, and Charlotte Oehl determined osmolalities. Special thanks go to Hans-Peter Bochem and the Institute of Bio- and Nanosystems 2 at Forschungszentrum Jülich for the liberal use of their SEM facilities, and to Ulrich Zimmermann for lending the xylem pressure probe setup. Many thanks go to Sigi Jahnke and Peter Blümler for critical discussion on many aspects of the work. We further thank both reviewers for their detailed and stimulating comments on the manuscript.

Received June 28, 2009; accepted November 29, 2009; published December 4, 2009.

LITERATURE CITED

Benkert R, Balling A, Zimmermann U (1991) Direct measurement of the pressure and flow in the xylem vessels of *Nicotiana tabacum* and their dependence on flow resistance and transpiration rate. Bot Acta **104:** 423–432

Biddulph O, Markle J (1944) Translocation of radiophosphorus in the phloem of the cotton plant. Am J Bot **31:** 65–70

Black JR, Epstein E, Rains WD, Yin QZ, Casey WH (2008) Magnesium-isotope fractionation during plant growth. Environ Sci Technol **42:** 7831–7836

Böhlke JK, de Laeter JR, De Bievre P, Hidaka H, Peiser HS, Rosman KJR, Taylor PDP (2005) Isotopic compositions of the elements, 2001. J Phys Chem Ref Data **34:** 57–67

Gilmer F, Schurr U (2007) Dynamic and nutrient fluxes in the xylem. *In* B Sattelmacher, WJ Horst, eds, The Apoplast of Higher Plants: Compartment of Storage, Transport, and Reactions. Springer, Dordrecht, The Netherlands, pp 221–229

Horst WJ, Kollmeier M, Schmohl N, Sivaguru M, Wang Y, Felle HH, Hedrich R, Schröder W, Staß A (2007) Significance of the root apoplast for aluminium toxicity and resistance of maize. *In* B Sattelmacher, WJ Horst, eds, The Apoplast of Higher Plants: Compartment of Storage, Transport, and Reactions. Springer, Dordrecht, The Netherlands, pp 49–66

Jeschke WD, Atkins CA, Pate JS (1985) Ion circulation via phloem and xylem between root and shoot of nodulated white lupin. J Plant Physiol **117:** 319–330

Jeschke WD, Hartung W (2000) Root-shoot interactions in mineral nutrition. Plant Soil **226:** 57–69

Jeschke WD, Pate JS (1991) Modeling of the partitioning, assimilation and storage of nitrate within root and shoot organs of castor bean (*Ricinus communis* L.). J Exp Bot **42:** 1091–1103

Koroleva OA, Davies A, Deeken R, Thorpe MR, Tomos AD, Hedrich R (2000) Identification of a new glucosinolate-rich cell type in Arabidopsis flower stalk. Plant Physiol **124:** 599–608

Kuhn AJ, Schroeder WH, Bauch J (2000) The kinetics of calcium and magnesium entry into mycorrhizal spruce roots. Planta **210:** 488–496

Lang A (1983) Turgor-regulated translocation. Plant Cell Environ **6:** 683–689

Leigh RA (2001) Potassium homeostasis and membrane transport. J Plant Nutr Soil Sci **164:** 193–198

Marschner H (1995) Mineral Nutrition of Higher Plants, Ed 2. Academic Press, London

Marschner H, Kirkby EA, Engels C (1997) Importance of cycling and recycling of mineral nutrients within plants for growth and development. Bot Acta **110:** 265–273

Metzner R, Schneider HU, Breuer U, Schroeder WH (2008) Imaging nutrient distributions in plant tissue using time-of-flight secondary ion mass spectrometry and scanning electron microscopy. Plant Physiol **147:** 1774–1787

Minchin PEH, Thorpe MR (1984) Apoplastic phloem unloading in the stem of bean. J Exp Bot **35:** 538–550

Pate JS, Layzell DB, McNeil DL (1979) Modeling the transport and utilization of carbon and nitrogen in a nodulated legume. Plant Physiol **63:** 730–737

Rygol J, Pritchard J, Zhu JJ, Tomos AD, Zimmermann U (1993) Transpiration induces radial turgor pressure gradients in wheat and maize roots. Plant Physiol **103:** 493–500

Schneider HU, Wegner LH, Haase A, Zimmermann U (2007) Long-distance water transport under controlled transpirational conditions: minimal-invasive investigations by means of pressure probes and NMR imaging. *In* B Sattelmacher, WJ Horst, eds, The Apoplast of Higher Plants: Compartment of Storage, Transport, and Reactions. Springer, Dordrecht, The Netherlands, pp 251–264

Siebrecht S, Herdel K, Schurr U, Tischner R (2003) Nutrient translocation in the xylem of poplar: diurnal variations and spatial distribution along the shoot axis. Planta **217:** 783–793

Stelzer R, Lehmann H, Kramer D, Luttge U (1990) X-ray microprobe analyses of vacuoles of spruce needle mesophyll, endodermis and transfusion parenchyma cells at different seasons of the year. Bot Acta **103:** 415–423

Stephan T, Zehnpfenning J, Benninghoven A (1994) Correction of dead-time effects in time-of-flight mass-spectrometry. J Vac Sci Technol A **12:** 405–410

Stout PR, Hoagland DR (1939) Upward and lateral movement of salt in certain plants as indicated by radioactive isotopes of potassium, sodium, and phosphorus absorbed by roots. Am J Bot **26:** 320–324

Szczerba MW, Britto DT, Kronzucker HJ (2006) Rapid, futile K^+ cycling and pool-size dynamics define low-affinity potassium transport in barley. Plant Physiol **141:** 1494–1507

Thompson MV, Zwieniecki MA (2005) The role of potassium in long distance transport in plants. *In* NM Holbrook, MA Zwieniecki, eds, Vascular Transport in Plants. Elsevier Publishing, San Diego, pp 221–240

Thürmer F, Zhu JJ, Gierlinger N, Schneider H, Benkert R, Gessner P, Herrmann B, Bentrup FW, Zimmermann U (1999) Diurnal changes in xylem pressure and mesophyll cell turgor pressure of the liana *Tetrastigma voinierianum*: the role of cell turgor in long-distance water transport. Protoplasma **206:** 152–162

van Bel AJE (1974) Absorption of L-alpha-alanine and L-alpha-amino-iso-butyric acid during their movement through xylem vessels of tomato stem segments. Acta Bot Neerl **23:** 305–313

van Bel AJE (1978) Free space of xylem translocation pathway of tomato stem. J Exp Bot **29:** 295–303

van Bel AJE (1990) Xylem-phloem exchange via the rays: the undervalued route of transport. J Exp Bot **41:** 631–644

van Bel AJE (2003) Transport phloem: low profile, high impact. Plant Physiol **131:** 1509–1510

van der Schoot C, van Bel AJE (1990) Mapping membrane potential differences and dye-coupling in internodal tissues of tomato (*Solanum lycopersicum* L.). Planta **182:** 9–21

van Ieperen W (2007) Ion-mediated changes of xylem hydraulic resistance *in planta*: fact or fiction? Trends Plant Sci **12:** 137–142

Wegner LH, Zimmermann U (2009) Hydraulic conductance and K^+ transport into the xylem depend on radial volume flow, rather than on xylem pressure, in roots of intact, transpiring maize seedlings. New Phytol **181:** 361–373

Wistuba N, Reich R, Wagner HJ, Zhu JJ, Schneider H, Bentrup FW, Haase A, Zimmermann U (2000) Xylem flow and its driving forces in a tropical liana: concomitant flow-sensitive NMR imaging and pressure probe measurements. Plant Biol **2:** 579–582

Wolf O, Munns R, Tonnet ML, Jeschke WD (1991) The role of the stem in the partitioning of Na^+ and K^+ in salt-treated barley. J Exp Bot **42:** 697–704

Wolterbeek HT, Vanluipen J, Debruin M (1985) Actual escape area and lateral escape from the xylem of the alkali ions Na^+, K^+, Rb^+ and Cs^+ in tomato. Physiol Plant **65:** 467–475

Zimmermann U, Rygol J, Balling A, Klock G, Metzler A, Haase A (1992) Radial turgor and osmotic-pressure profiles in intact and excised roots of *Aster tripolium*: pressure probe measurements and nuclear magnetic-resonance-imaging analysis. Plant Physiol **99:** 186–196